http://www.applmathmech.cn

基于分层法的功能梯度三明治壳线性弯曲无网格分析*

陈　卫[1]，　汤智宏[1]，　彭林欣[2]

（1. 南华大学 土木工程学院，湖南 衡阳 421001；
2. 广西大学 土木建筑工程学院，南宁 530004）

摘要： 基于 3D 连续壳理论和一阶剪切变形理论，采用分层法，提出了一种求解功能梯度三明治壳线性弯曲问题的移动最小二乘无网格法.通过映射技术，将随动坐标系上的二维无网格节点信息映射到三维壳中，并在随动坐标系上形成移动最小二乘近似的形函数.因基于 3D 连续壳理论的壳数值解答无法像特定壳一样给出其厚度方向的显式表达式，该文将功能梯度三明治材料壳结构中材料参数变化的部分划分成若干层，得到每层的材料参数为常数.利用最小势能原理，推导出了功能梯度三明治壳线性弯曲的无网格控制方程.通过引入一个厚度方向的线性变换，使得每层厚度方向的 Gauss 积分均在−1 至 1 区间内，不违背一阶剪切变形理论.采用完全转化法施加本质边界条件.以功能梯度三明治板、柱壳、双曲扁壳经典几何形状壳为例，讨论了不同梯度系数、径厚比和曲率半径等对数值结果的影响，并将计算结果与文献解对比.研究表明，该方法在求解不同形状的功能梯度三明治壳线性弯曲问题时，具有收敛性好、计算精度高的特点.

关　键　词： 分层法；　无网格法；　映射技术；　功能梯度三明治壳；　线性弯曲
中图分类号： O342　　**文献标志码：** A　　DOI：10.21656/1000-0887.440262

Linear Bending Analysis of Functionally Graded Sandwich Shells With the Meshless Method Based on the Layer-Wise Theory

CHEN Wei[1]，　TANG Zhihong[1]，　PENG Linxin[2]

（1. *School of Civil Engineering*, *University of South China*, *Hengyang*, *Hunan* 421001, *P.R.China*;
2. *School of Civil Engineering and Architecture*, *Guangxi University*, *Nanning* 530004, *P.R.China*）

Abstract: Based on the 3D continuous shell theory and the 1st-order shear deformation theory, a moving least squares meshless method was proposed for solving the linear bending problem of functionally graded sandwich shells with the layered method. With the mapping technology, the 2D meshless node information on the convected coordinate system was mapped on the 3D shell, and the shape function of moving least squares (MLS) approximation was formed on the convected coordinate system. Due to the inability of shell numerical solutions based on the 3D continuous shell theory to provide an explicit expression for the thickness direction of a specif-

* **收稿日期：** 2023-08-29；**修订日期：** 2023-12-15
基金项目： 国家自然科学基金(12162004;11562001)
作者简介： 陈卫(1991—)，男，讲师，博士，硕士生导师(E-mail：chenwei@usc.edu.cn)；
彭林欣(1977—)，男，教授，博士，博士生导师(通讯作者. E-mail：penglx@gxu.edu.cn).
引用格式： 陈卫，汤智宏，彭林欣. 基于分层法的功能梯度三明治壳线性弯曲无网格分析[J]. 应用数学和力学，2024，**45**(5)：539-553.

ic shell, the portion of material parameter changes in the functionally graded sandwich material shell structure was divided into several layers, and the material parameters of each layer were obtained as constants. The governing meshless equation for linear bending of functionally graded sandwich shells was derived under the principle of minimum potential energy. Through introduction of a linear transformation in the thickness direction, the Gaussian integral in the thickness direction of each layer was bounded within the range of −1 to 1, without violation of the 1st-order shear deformation theory (FSDT). The essential boundary conditions were employed with the complete transformation method. Finally, the effects of different gradient coefficients, diameter to thickness ratios, and curvature radii on numerical results were discussed through examples of functionally graded sandwich plates, cylindrical shells, and hyperbolic shallow shells with classical geometric shapes. The calculated results were compared with the literature solutions. The results show that, the proposed method has the characteristics of good convergence and high computation accuracy in solving linear bending problems of functional graded sandwich shells with different shapes.

Key words: layer-wise method; meshless method; mapping technology; functionally graded sandwich shell; linear bending

0 引 言

功能梯度材料(functionally graded material, FGM)是日本学者平井敏雄等针对航天技术中的高落差温度问题而提出的一种新型非均匀复合材料[1].FGM 各组分材料在空间位置上的连续变化使得材料内部功能的渐变,可以有效避免或降低应力集中等问题.功能梯度板壳以其优越的性能,掀起了学者们的研究热潮[2-3],并被广泛推广到航空航天、车辆、海洋等工程领域的应用中.

在功能梯度壳解析解方面,板作为一种特殊简单的壳形式,其解析解发展相对比较成熟[4-6].而对于壳体的解析解因其涉及到复杂的几何方程及 Lamé 系数等,相比板而言较少[7].数值计算方面,诸多学者采用了有限元法(finite element method,FEM)[8]、微分求积法(differential quadrature method,DQM)[9]、等几何分析(isogeometry analysis,IGA)[10]等方法分析了功能梯度(三明治)板壳的线性弯曲问题.

针对功能梯度板的平面断裂问题,黄干云和汪越胜等[11-12]将梯度材料划分成若干层,假设每层的弹性模量按线性函数变化,提出了分层模型,借助 Fourier 积分技术和传递矩阵方法,计算了界面裂纹应力强度因子.此后,黄立新等[13]、Nikbakht 等[14]同样将梯度材料划分成若干层,但他们假设每层的弹性模量为常数,采用 FEM 研究了功能梯度板的线性弯曲及自由振动问题.Brischetto[15]采用 3D 分层模型和几何规则壳(含 Lamé 系数项),给出了功能梯度三明治壳线性弯曲问题的解析解.

无网格作为一种兴起的数值方法,不需要像有限元那样划分网格和单元,且容易构造高阶形函数,避免了剪切、薄膜锁死.在国内,龙述尧等[16]采用无网格局部径向点插值法研究了功能梯度板的静力问题,邵玉龙等[17]采用二阶一致无网格法分析了功能梯度梁及厚壁圆筒的弯曲问题.在国外,在功能梯度板方面,诸多学者采用局部 Petrov 法(local Petrov-Galerkin method,LPGM)、径向点插值(radial point interpolation,RPI)、核粒子-Ritz(kernel particle-Ritz,kp-Ritz)、移动 Kriging 插值(moving Kriging,MK)等[18-22]方法研究了功能梯度(三明治)板的弯曲问题.在以上研究中,除了采用不同无网格方法外,部分还采用了不同的横向剪切变形理论.如一阶剪切变形理论(first order deformation theory,FSDT),简单的一阶剪切变形理论(simple-first order deformation theory,S-FSDT),高阶剪切变形理论(higher order deformation theory,HSDT),逆正弦剪切变形理论(inverse sin shear deformation theory,ISSDT)等.在功能梯度壳方面,Sladek 等[23]采用 LPGM,结合 MLS 求解了功能梯度双曲壳的线性弯曲与受迫振动问题.Zhao 等[24-25]采用 kp-Ritz 无网格方法研究了热环境下,功能梯度浅柱壳的线性弯曲、自由振动与屈曲问题.Zhao 等[26]基于 kp-Ritz 无网格方法研究了功能梯度锥壳的自由振动问题.Mellouli 等[27]基于几何精确壳理论[28],采用 RPI 研究了功能梯度壳的线性弯曲问题.Wang 等[29]采用 RPI 研究了面内材料不均匀的功能梯度壳静力和动力问题.

本文将功能三明治梯度材料中材料参数变化的部分划分成若干层,设定每层的弹性模量为常数,基于 3D 连续壳理论[30],提出了一种求解功能梯度三明治壳线性弯曲问题的移动最小二乘近似的无网格法.后文

中选用了几个不同形状的功能梯度三明治板壳算例,将本文计算结果与文献解对比,以此来验证本文方法计算功能梯度三明治壳线性弯曲的有效性及准确性.

1　几 何 模 型

直角坐标系与随动坐标系的关系如图 1 所示.$\boldsymbol{X}=(x,y,z)$ 是在直角坐标系中的位置矢量,$\boldsymbol{r}=(r_1,r_2,r_3)$ 是随动坐标系中的位置矢量,$\boldsymbol{e}_i$ 是直角坐标系中正交单位矢量,$\boldsymbol{V}_i$ 是壳中面某一点的正交单位矢量.根据 Mindlin 板壳理论,壳上任意一点的位置及位移矢量参数可分别表示为

$$\boldsymbol{X}=\boldsymbol{X}_{\mathrm{mid}}+\frac{r_3}{2}h\boldsymbol{V}_3(r_1,r_2), \tag{1}$$

$$\boldsymbol{u}=\boldsymbol{u}_{\mathrm{mid}}+\frac{r_3}{2}h(-\theta_1\boldsymbol{V}_2+\theta_2\boldsymbol{V}_1), \tag{2}$$

式中,$\boldsymbol{X}_{\mathrm{mid}}$ 是壳中面的点在直角坐标系中的位置矢量,h 为厚度,r_1,r_2 是壳中面内的参数,r_3 是厚度方向的参数,$\boldsymbol{u}_{\mathrm{mid}}(u,v,w)$ 是壳中面的点在直角坐标系中的位移,θ_1,θ_2 分别为绕壳中面正交矢量 $\boldsymbol{V}_1,\boldsymbol{V}_2$ 的转角,$\boldsymbol{V}_3$ 是垂直壳中面的单位法向矢量,$\boldsymbol{V}_1,\boldsymbol{V}_2,\boldsymbol{V}_3$ 有如下关系:

$$\boldsymbol{V}_2=\frac{\boldsymbol{V}_3\times\boldsymbol{e}_1}{|\boldsymbol{V}_3\times\boldsymbol{e}_1|},\ \boldsymbol{V}_1=\boldsymbol{V}_2\times\boldsymbol{V}_3. \tag{3}$$

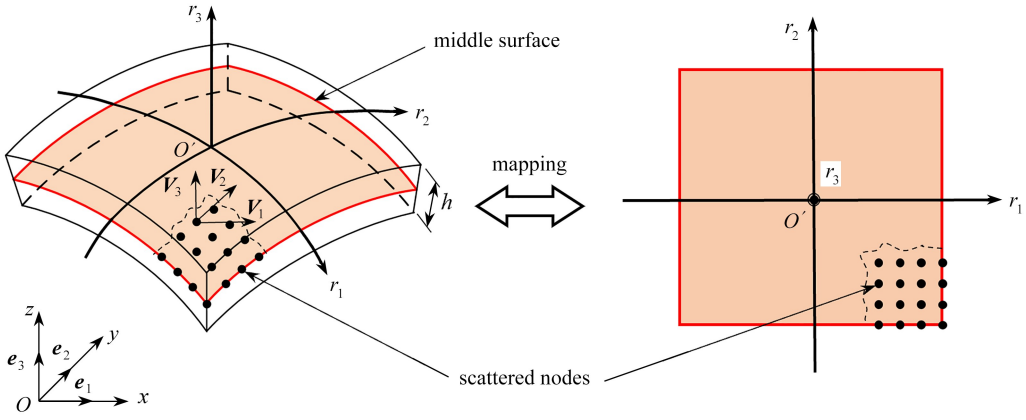

(a) 直角坐标系　　(b) 随动坐标系

(a) The Cartesian coordinate system　　(b) The convected coordinate system

图 1　曲壳无网格几何模型及映射技术

Fig. 1　The meshless geometric model for the curved shell and the mapping technique

2　数 学 模 型

2.1　形函数

由移动最小二乘近似[31]给出功能梯度壳中面第 I 个节点在随动坐标系上的形函数:

$$N_I(r_1,r_2)=\boldsymbol{q}^{\mathrm{T}}(r_1,r_2)\boldsymbol{B}^{-1}(r_1,r_2)\boldsymbol{q}(r_{1I},r_{2I})\bar{\omega}(r_1-r_{1I},r_2-r_{2I}), \tag{4}$$

式中,$\boldsymbol{B}(r_1,r_2)=\sum_{I=1}^{n}\bar{\omega}(r_1-r_{1I},r_1-r_{2I})\boldsymbol{q}(r_{1I},r_{2I})\boldsymbol{q}^{\mathrm{T}}(r_1,r_2)$,$\boldsymbol{q}^{\mathrm{T}}(r_1,r_2)=[1,r_1,r_2,r_1^2,r_1r_2,r_2^2]$ 为二次基($m=6$),$\bar{\omega}$ 为权函数,本文取三次样条权函数:

$$\bar{\omega}(r)=\begin{cases}2/3-4r^2+4r^3, & r\leqslant 1/2,\\ 4/3-4r+4r^2-4r^3/3, & 1/2<r\leqslant 1,\\ 0, & r>1.\end{cases} \tag{5}$$

2.2　位移场近似

根据式(4),利用移动最小二乘近似逼近式(1)、(2),则有

$$\boldsymbol{X}(\boldsymbol{r}) = \sum_{I=1}^{n} N_I(r_1, r_2)\left(\boldsymbol{X}_{\mathrm{mid}I} + \frac{r_3}{2} h\boldsymbol{V}_3\right), \tag{6}$$

$$\boldsymbol{u}(\boldsymbol{r}) = \sum_{I=1}^{n} N_I(r_1, r_2)\left(\boldsymbol{u}_{\mathrm{mid}I} + \frac{r_3}{2} h(-\theta_{1I}\boldsymbol{V}_2 + \theta_{2I}\boldsymbol{V}_1)\right). \tag{7}$$

式(6)、(7)改写成矩阵形式,分别为

$$\boldsymbol{X}(\boldsymbol{r}) = \begin{bmatrix} x \\ y \\ z \end{bmatrix} = \sum_{I=1}^{n} N_I(r_1, r_2) \begin{bmatrix} x_I + (h/2) r_3 V_{3(1)} \\ y_I + (h/2) r_3 V_{3(2)} \\ z_I + (h/2) r_3 V_{3(3)} \end{bmatrix}, \tag{8}$$

$$\boldsymbol{u}(\boldsymbol{r}) = \begin{bmatrix} u \\ v \\ w \end{bmatrix} = \sum_{I=1}^{n} \begin{bmatrix} N_I & 0 & 0 & -\dfrac{h}{2} r_3 N_I V_{2(1)} & \dfrac{h}{2} r_3 N_I V_{1(1)} \\ 0 & N_I & 0 & -\dfrac{h}{2} r_3 N_I V_{2(2)} & \dfrac{h}{2} r_3 N_I V_{1(2)} \\ 0 & 0 & N_I & -\dfrac{h}{2} r_3 N_I V_{2(3)} & \dfrac{h}{2} r_3 N_I V_{1(3)} \end{bmatrix} \begin{bmatrix} u_I \\ v_I \\ w_I \\ \theta_{1I} \\ \theta_{2I} \end{bmatrix}, \tag{9}$$

式中,$[u_I, v_I, w_I, \theta_{1I}, \theta_{2I}]^{\mathrm{T}} = \boldsymbol{U}_I$ 是壳中面上第 I 个节点的节点参数,n 是壳中面节点个数.

式(6)的位置矢量对随动坐标系 r_i 求偏导,可得到协变基矢量 $\boldsymbol{g}_i(i = 1,2,3)$ 为

$$\boldsymbol{g}_i = \frac{\partial \boldsymbol{X}(\boldsymbol{r})}{\partial r_i}. \tag{10}$$

将上式展开有

$$\begin{cases} \dfrac{\partial \boldsymbol{X}(\boldsymbol{r})}{\partial r_i} = \displaystyle\sum_{I=1}^{n} \frac{\partial N_I(r_1, r_2)}{\partial r_i}\left(\boldsymbol{X}_{\mathrm{mid}I} + \frac{r_3}{2} h\boldsymbol{V}_3\right), & i = 1,2, \\ \dfrac{\partial \boldsymbol{X}(\boldsymbol{r})}{\partial r_3} = \displaystyle\sum_{I=1}^{n} N_I(r_1, r_2)\ \frac{1}{2} h\boldsymbol{V}_3. \end{cases} \tag{11}$$

整理式(11),可得 Jacobi 矩阵为

$$\boldsymbol{J} = \begin{Bmatrix} \boldsymbol{g}_1^{\mathrm{T}} \\ \boldsymbol{g}_2^{\mathrm{T}} \\ \boldsymbol{g}_3^{\mathrm{T}} \end{Bmatrix} = \begin{bmatrix} \dfrac{\partial x}{\partial r_1} & \dfrac{\partial y}{\partial r_1} & \dfrac{\partial z}{\partial r_1} \\ \dfrac{\partial x}{\partial r_2} & \dfrac{\partial y}{\partial r_2} & \dfrac{\partial y}{\partial r_2} \\ \dfrac{\partial x}{\partial r_3} & \dfrac{\partial y}{\partial r_3} & \dfrac{\partial z}{\partial r_3} \end{bmatrix}. \tag{12}$$

2.3 位移-应变关系

根据移动最小二乘近似,壳中面上任意一点的向量 $\boldsymbol{V}_i$ 可表示为

$$\boldsymbol{V}_i = \frac{\displaystyle\sum_{I=1}^{n} N_I(r_1, r_2)\boldsymbol{V}_{Ii}}{\left|\displaystyle\sum_{I=1}^{n} N_I(r_1, r_2)\boldsymbol{V}_{Ii}\right|}, \qquad i = 2,3,\ \boldsymbol{V}_1 = \boldsymbol{V}_2 \times \boldsymbol{V}_3, \tag{13}$$

式中,$\boldsymbol{V}_{Ii}$ 为第 I 个节点的 $\boldsymbol{V}_i$ 矢量.

将式(7)对随动坐标 r_i 求偏导,可得:

当 $j = 1,2$ 时,

$$\frac{\partial \boldsymbol{u}}{\partial r_i} = \sum_{I=1}^{n} \left\{ \frac{\partial N_I}{\partial r_i} \boldsymbol{u}_{\mathrm{mid}I} + \frac{r_3}{2} h\left[\left(-\frac{\partial N_I}{\partial r_i} \boldsymbol{V}_2 - N_I \frac{\partial \boldsymbol{V}_2}{\partial r_i} \right) \theta_{1I} + \left(\frac{\partial N_I}{\partial r_i} \boldsymbol{V}_1 + N_I \frac{\partial \boldsymbol{V}_1}{\partial r_i} \right) \theta_{2I} \right] \right\}; \tag{14}$$

当 $j = 3$ 时,

$$\frac{\partial \boldsymbol{u}}{\partial r_3} = \sum_{I=1}^{n} N_I \frac{1}{2} h(-\boldsymbol{V}_2\theta_{1I} + \boldsymbol{V}_1\theta_{2I}). \tag{15}$$

式(14)和式(15)改写成矩阵形式,分别为:

当 $j=1,2$ 时,

$$\frac{\partial \boldsymbol{u}}{\partial r_j}=\sum_{I=1}^{n}\begin{bmatrix}\dfrac{\partial N_I}{\partial r_j} & 0 & 0\\ 0 & \dfrac{\partial N_I}{\partial r_j} & 0\\ 0 & 0 & \dfrac{\partial N_I}{\partial r_j}\end{bmatrix}\begin{Bmatrix}u_I\\ v_I\\ w_I\end{Bmatrix}+$$

$$\sum_{I=1}^{n}\begin{bmatrix}-\dfrac{r_3}{2}hV_{2(1)}\dfrac{\partial N_I}{\partial r^j}-\dfrac{r_3}{2}h\dfrac{\partial V_{2(1)}}{\partial r^j}N_I & \dfrac{r_3}{2}hV_{1(1)}\dfrac{\partial N_I}{\partial r^j}+\dfrac{r_3}{2}h\dfrac{\partial V_{1(1)}}{\partial r^j}N_I\\ -\dfrac{r_3}{2}hV_{2(2)}\dfrac{\partial N_I}{\partial r^j}-\dfrac{r_3}{2}h\dfrac{\partial V_{2(2)}}{\partial r^j}N_I & \dfrac{r_3}{2}hV_{1(2)}\dfrac{\partial N_I}{\partial r^j}+\dfrac{r_3}{2}h\dfrac{\partial V_{1(2)}}{\partial r^j}N_I\\ -\dfrac{r_3}{2}hV_{2(3)}\dfrac{\partial N_I}{\partial r^j}-\dfrac{r_3}{2}h\dfrac{\partial V_{2(3)}}{\partial r^j}N_I & \dfrac{r_3}{2}hV_{1(3)}\dfrac{\partial N_I}{\partial r^j}+\dfrac{r_3}{2}h\dfrac{\partial V_{1(3)}}{\partial r^j}N_I\end{bmatrix}\begin{Bmatrix}\theta_{1I}\\ \theta_{2I}\end{Bmatrix}=$$

$$\sum_{I=1}^{n}\begin{bmatrix}\boldsymbol{\alpha}_{j1} & \boldsymbol{\alpha}_{j2} & \boldsymbol{\alpha}_{j3}\end{bmatrix}\begin{Bmatrix}u_I\\ v_I\\ w_I\end{Bmatrix}+\sum_{I=1}^{n}\begin{bmatrix}\boldsymbol{b}_{1i,j} & \boldsymbol{b}_{2i,j}\end{bmatrix}\begin{Bmatrix}\theta_{1I}\\ \theta_{2I}\end{Bmatrix};\tag{16}$$

当 $j=3$ 时,

$$\frac{\partial \boldsymbol{u}}{\partial r_3}=\sum_{I=1}^{n}\begin{bmatrix}-\dfrac{1}{2}hV_{2(1)}N_I & -\dfrac{1}{2}hV_{1(1)}N_I\\ -\dfrac{1}{2}hV_{2(2)}N_I & -\dfrac{1}{2}hV_{1(2)}N_I\\ -\dfrac{1}{2}hV_{2(3)}N_I & -\dfrac{1}{2}hV_{1(3)}N_I\end{bmatrix}\begin{Bmatrix}\theta_{1I}\\ \theta_{2I}\end{Bmatrix}=\sum_{I=1}^{n}\begin{bmatrix}\boldsymbol{c}_{1i} & \boldsymbol{c}_{2i}\end{bmatrix}\begin{Bmatrix}\theta_{1I}\\ \theta_{2I}\end{Bmatrix},\tag{17}$$

式中, $\partial \boldsymbol{V}_i/\partial r_j$ 为

$$\frac{\partial \boldsymbol{V}_i}{\partial r_j}=(\boldsymbol{I}-\boldsymbol{V}_i\otimes\boldsymbol{V}_i)\Delta\boldsymbol{V}_{ij},\ \Delta\boldsymbol{V}_{ij}=\frac{\sum_{I=1}^{n}(\partial N_I/\partial r_j)\boldsymbol{V}_{Ii}}{\left|\sum_{I=1}^{n}N_I\boldsymbol{V}_{Ii}\right|},\qquad i=2,3,\ j=1,2,\tag{18}$$

$$\frac{\partial \boldsymbol{V}_1}{\partial r_j}=\frac{\partial \boldsymbol{V}_2}{\partial r_j}\times\boldsymbol{V}_3+\boldsymbol{V}_2\times\frac{\partial \boldsymbol{V}_3}{\partial r_j},\qquad j=1,2,\tag{19}$$

其中, $\boldsymbol{I}$ 为 3×3 单位矩阵.

小位移分析应变张量为

$$\boldsymbol{\varepsilon}_{ij}=\frac{1}{2}\left(\frac{\partial \boldsymbol{u}}{\partial x^j}+\frac{\partial \boldsymbol{u}}{\partial x^i}\right)=\frac{1}{2}\left(\frac{\partial \boldsymbol{u}}{\partial r_j}\boldsymbol{J}_{ij}^{-1}+\frac{\partial \boldsymbol{u}}{\partial r_i}\boldsymbol{J}_{ji}^{-1}\right).\tag{20}$$

将式(12)、(16)和(17)代入式(20)可得到应变张量如下:

$$\boldsymbol{\varepsilon}=\begin{Bmatrix}\varepsilon_{11}\\ \varepsilon_{22}\\ \varepsilon_{33}\\ 2\varepsilon_{12}\\ 2\varepsilon_{23}\\ 2\varepsilon_{31}\end{Bmatrix}=\sum_{I=1}^{n}\begin{bmatrix}N_{,1} & 0 & 0 & G_{1,1}^1 & G_{1,1}^2\\ 0 & N_{,2} & 0 & G_{2,2}^1 & G_{2,2}^2\\ 0 & 0 & N_{,3} & G_{3,3}^1 & G_{3,3}^2\\ N_{,2} & N_{,1} & 0 & G_{1,2}^1+G_{2,1}^1 & G_{1,2}^2+G_{2,1}^2\\ 0 & N_{,3} & N_{,2} & G_{2,3}^1+G_{3,2}^1 & G_{2,3}^2+G_{3,2}^2\\ N_{,3} & 0 & N_{,1} & G_{1,3}^1+G_{3,1}^1 & G_{1,3}^2+G_{3,1}^2\end{bmatrix}\begin{Bmatrix}u_I\\ v_I\\ w_I\\ \theta_{1I}\\ \theta_{2I}\end{Bmatrix}=\sum_{I=1}^{n}\boldsymbol{B}_I\boldsymbol{U}_I,\tag{21}$$

式中，$N_{,i}=\boldsymbol{J}_{i1}^{-1}\dfrac{\partial N}{\partial r_1}+\boldsymbol{J}_{i2}^{-1}\dfrac{\partial N}{\partial r_2}$，$\boldsymbol{G}_{i,j}^{k}=\boldsymbol{b}_{ki,1}\boldsymbol{J}_{j1}^{-1}+\boldsymbol{b}_{ki,2}\boldsymbol{J}_{j2}^{-1}+\boldsymbol{c}_{ki}\boldsymbol{J}_{j3}^{-1}$，$\boldsymbol{J}_{ij}^{-1}$ 中的 i 和 j 分别表示 Jacobi 矩阵的逆矩阵中元素所在的行和列.

2.4 本构模型

假定材料常数沿厚度方向遵循如下规律变化：

$$P(z)=(P_{\mathrm{c}}-P_{\mathrm{m}})V_{\mathrm{c}}(z)+P_{\mathrm{m}}, \tag{22}$$

式中，P 表示材料的物理参数，如弹性模量 E 和 Poisson 比 ν 等，由于 Poisson 比变化不大，可假定为常数；下标 m 和 c 分别代表金属和陶瓷；$V_{\mathrm{c}}(z)$ 为体积分数.

根据体积分数分布不同，本文考虑如下 3 种类型的功能梯度壳(图 2)：

Type A：功能梯度壳

$$V_{\mathrm{c}}(z)=\left(\frac{2z+h}{2h}\right)^{p},\qquad z\in\left[-\frac{h}{2},\frac{h}{2}\right]. \tag{23}$$

Type B：功能梯度芯夹层壳

$$\begin{cases}V_{\mathrm{c}}^{(1)}(z)=0, & z\in[h_0,h_1],\\ V_{\mathrm{c}}^{(2)}(z)=\left(\dfrac{z-h_1}{h_2-h_1}\right)^{p}, & z\in[h_1,h_2],\\ V_{\mathrm{c}}^{(3)}(z)=1, & z\in[h_2,h_3].\end{cases} \tag{24}$$

Type C：功能梯度面板夹层壳

$$\begin{cases}V_{\mathrm{c}}^{(1)}(z)=\left(\dfrac{z-h_0}{h_1-h_0}\right)^{p}, & z\in[h_0,h_1],\\ V_{\mathrm{c}}^{(2)}(z)=1, & z\in[h_1,h_2],\\ V_{\mathrm{c}}^{(3)}(z)=\left(\dfrac{z-h_3}{h_2-h_3}\right)^{p}, & z\in[h_2,h_3].\end{cases} \tag{25}$$

式(23)—(25)中，p 为梯度指数.

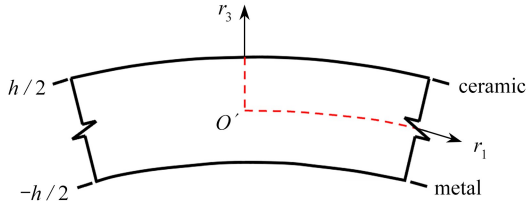

(a) Type A

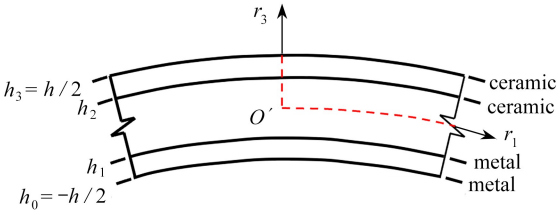

(b) Type B

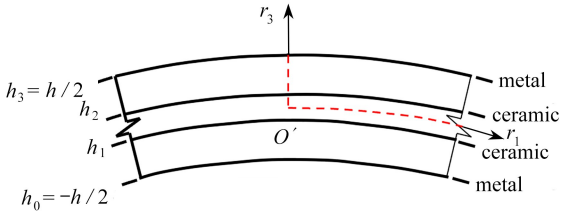

(c) Type C

图 2 3 类功能梯度壳

Fig. 2 Three types of functionally graded shells

由于壳体本构关系是定义在随动坐标系上，需根据虚功原理变换到直角坐标系上，则有

$$\boldsymbol{\sigma}=(\boldsymbol{T}_{\varepsilon}^{\mathrm{T}}\boldsymbol{D}'\boldsymbol{T}_{\varepsilon})\boldsymbol{\varepsilon}=\boldsymbol{D}\boldsymbol{\varepsilon}, \tag{26}$$

其中

$$\boldsymbol{T}_{\varepsilon}=\begin{bmatrix} l_1^2 & m_1^2 & n_1^2 & l_1m_1 & m_1n_1 & n_1l_1 \\ l_2^2 & m_2^2 & n_2^2 & l_2m_2 & m_2n_2 & n_2l_2 \\ 2l_1l_2 & 2m_1m_2 & 2n_1n_2 & l_1m_2+l_2m_1 & m_1n_2+m_2n_1 & n_1l_2+n_2l_1 \\ 2l_2l_3 & 2m_2m_3 & 2n_2n_3 & l_2m_3+l_2m_3 & m_2n_3+m_2n_3 & n_2l_3+n_2l_3 \\ 2l_3l_1 & 2m_3m_1 & 2n_3n_1 & l_3m_1+l_3m_1 & m_3n_1+m_3n_1 & n_3l_1+n_3l_1 \end{bmatrix},$$

$$\boldsymbol{D}'=\frac{E(z)}{1-\nu^2}\begin{bmatrix} 1 & \nu & 0 & 0 & 0 \\ & 1 & 0 & 0 & 0 \\ & & \dfrac{1-\nu}{2} & 0 & 0 \\ & \text{sym} & & \dfrac{1-\nu}{2K_s} & 0 \\ & & & & \dfrac{1-\nu}{2K_s} \end{bmatrix},$$

式中, l_i, m_i, n_i 分别为局部正交单位矢量 $\boldsymbol{V}_i(i=1,2,3)$ 的三个分量, $K_s=6/5$ 为剪切修正因子.

2.5　控制方程

功能梯度三明治壳在径向均布荷载作用下的能量泛函为

$$\Pi_B=\frac{1}{2}\iiint\boldsymbol{\varepsilon}^T\boldsymbol{D}\boldsymbol{\varepsilon}\mathrm{d}x\mathrm{d}y\mathrm{d}z-\iint qw\mathrm{d}x\mathrm{d}y. \tag{27}$$

将式(9)代入上式,并结合应力-应变方程式(26),可得

$$\Pi_B=\frac{1}{2}\boldsymbol{U}^T\boldsymbol{K}\boldsymbol{U}-\boldsymbol{U}\boldsymbol{F}, \tag{28}$$

其中

$$\boldsymbol{K}=\int_V\boldsymbol{B}_I^T\boldsymbol{D}\boldsymbol{B}_I\mathrm{d}V=\int_V\boldsymbol{B}_I^T\boldsymbol{D}\boldsymbol{B}_I|J|\mathrm{d}r_1\mathrm{d}r_2\mathrm{d}r_3, \tag{29}$$

$$\boldsymbol{F}=\iint[V_{3(1)}\quad V_{3(2)}\quad V_{3(3)}\quad 0\quad 0]^TN_Iq\frac{|\boldsymbol{J}'|}{V_{3(3)}}\mathrm{d}r^1\mathrm{d}r^2, \tag{30}$$

式中, $\boldsymbol{J}'$ 为 Jacobi 矩阵 $\boldsymbol{J}$ 的前两行两列.

为了应用 Gauss 积分,且不违反一阶剪切变形理论,通过如下线性变换使得每层功能梯度三明治壳的厚度方向积分为-1 到 1,表达形式如下:

$$r_3=-1+\left[2\sum_{j=1}^{k}h_j-h_k(1-r_3^k)\right]/h. \tag{31}$$

将式(31)代入式(29),可得基于分层法的功能梯度三明治壳的刚度矩阵:

$$\boldsymbol{K}=\sum_{k=1}^{N_L}\int_V\boldsymbol{B}_I^T\boldsymbol{D}\boldsymbol{B}_I(h_k/h)|\boldsymbol{J}|\mathrm{d}r_1\mathrm{d}r_2\mathrm{d}r_3^k, \tag{32}$$

式中, N_L 为总分层数.

根据最小势能原理,由 $\Pi_B=0$, 可得功能梯度三明治壳线性弯曲控制方程为

$$\boldsymbol{K}\boldsymbol{U}=\boldsymbol{F}. \tag{33}$$

3　完全转换法

基于移动最小二乘近似的无网格法不满足 Kronecker 条件, 控制方程(33)的未知量是节点参数而非真实位移, 不能像有限元法那样直接施加本质边界条件, 本文采用 Chen 等[32]提出的完全转换法来修正刚度方程:

$$\bar{\boldsymbol{K}}\bar{\boldsymbol{U}}=\bar{\boldsymbol{F}}, \tag{34}$$

式中，$\boldsymbol{U}$ 是真实节点位移，$\bar{\boldsymbol{K}}=\boldsymbol{T}^{\mathrm{T}}\boldsymbol{K}\boldsymbol{T}$，$\bar{\boldsymbol{F}}=\boldsymbol{T}^{\mathrm{T}}\boldsymbol{F}$，$\boldsymbol{T}$ 的表达式为

$$\boldsymbol{T}=\boldsymbol{\Lambda}^{-1}=\begin{bmatrix} N_1(\boldsymbol{r}_1) & N_2(\boldsymbol{r}_1) & \cdots & N_n(\boldsymbol{r}_1) \\ N_1(\boldsymbol{r}_2) & N_2(\boldsymbol{r}_2) & \cdots & N_n(\boldsymbol{r}_2) \\ \vdots & \vdots & & \vdots \\ N_1(\boldsymbol{r}_n) & N_2(\boldsymbol{r}_n) & \cdots & N_n(\boldsymbol{r}_n) \end{bmatrix}^{-1}. \tag{35}$$

4 算 例 分 析

所有算例中影响域均采用方形，定义 $h_{r1}=d_{\max}\times c_{r1}$，$h_{r2}=d_{\max}\times c_{r2}$．$h_{r1}$ 和 h_{r2} 分别为影响域 r_1 和 r_2 方向的长度，c_{r1} 和 c_{r2} 分别为 r_1 和 r_2 方向两个相邻节点的距离，取 $d_{\max}=3$．采用背景网格积分，每个网格内 Gauss 积分点为 3×3，每层厚度方向 Gauss 积分点数为 2．材料属性见表 1．每个算例中均采用不同均匀布置的离散节点方案及层数进行收敛性分析，并将计算结果与文献解进行对比．中点挠度无量纲化公式如下：

$$\bar{w}^1=\frac{10w_{\mathrm{c}}E_{\mathrm{c}}h^3}{qa^4},\ \bar{w}^2=\frac{10w_{\mathrm{c}}E_0h}{qa^2},\ E_0=1\ \mathrm{GPa},\ \bar{w}^3=\frac{w_{\mathrm{c}}}{h},\ \bar{w}^4=\frac{100w_{\mathrm{c}}E_{\mathrm{c}}h^3}{qa^4}.$$

本文考虑常见的 3 种边界条件，以 $r_1=0$ 边界为例有：

① 固支(clamp，C)：$u=v=w=\theta_1=\theta_2=0$；

② 简支(simply，S)：$N_x=M_x=v=w=\theta_2=0$；

③ 自由(free，F)：无约束．

表 1 功能梯度材料组成元素

Table 1 Properties of the FGM components

property	Al	ceramic	
		Al_2O_3	ZrO_2
E/GPa	70	380	200
ν	0.3	0.3	0.3

4.1 剪切锁死

将 FGM 板退化为各向同性板，设一承受横向均布荷载 $P=1\ \mathrm{N/m^2}$ 的四边固支方板尺寸为 20 m × 20 m × 1 m，弹性模量 $E=10\ 000\ \mathrm{N/m^2}$，Poisson 比 $\nu=0.499\ 99$(近似为不可压缩材料)．图 3 给出了不同无网格节点数下方板挠度结果与解析解[33]的对比曲线，可以看出本文方法具有较好的收敛性．为观察剪切锁死，设 $\nu=0.3$，其他参数同上．图 4 给出了当 $b/h=10,100,1\ 000$，基函数分别为二次基($m=6$)、三次基($m=10$)、四次基($m=15$) 和双三次基($m=16$)，在 14 × 14 无网格节点数下方板中点的收敛性情况，可以看出 $b/h=1\ 000$ 的薄板，采取双三次基函数能够避免剪切锁死现象．

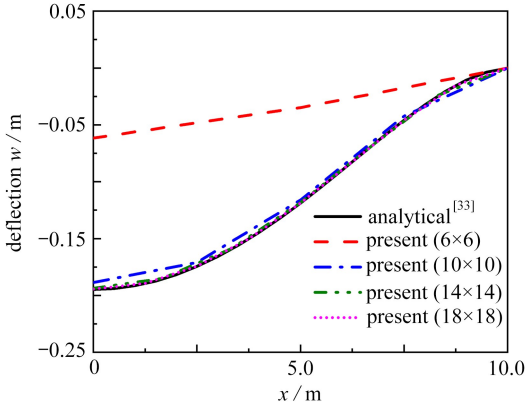

图 3 不同节点数下方板挠度分析结果

Fig. 3 Analysis results of plate deflections under different node numbers

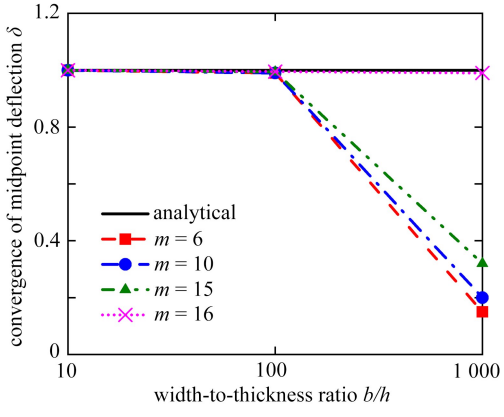

图 4 不同宽厚比下方板中点收敛性分析

Fig. 4 Convergence analysis of the midpoint of the plate under different width-to-thickness ratios

4.2　Type B 和 Type C 方板

如图 5 所示,考虑四边简支的 Type B 和 Type C 方板,宽厚比 $b/h = 10$,荷载类型为正弦荷载 $q(r_1, r_2) = q\sin(\pi r_1/a)\sin(\pi r_2/b)$.Type B 方板厚度为 1-8-1,即上下表层为 $0.1h$,中间核为 $0.8h$.Type C 方板考虑 5 种层状厚度分布类型.对于弹性模量不变的厚度部分,如 Type B 中的上下表层,采用一层计算即可.

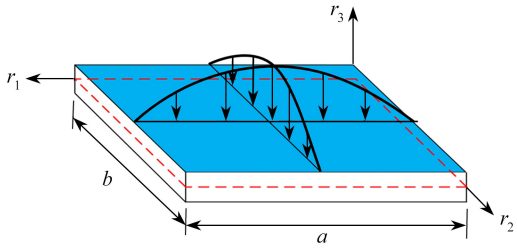

图 5　功能梯度方板受正弦荷载示意图

Fig. 5　Schematic diagram of a functionally graded square plate under uniformly distributed load

表 2 给出了梯度指数为 10 不同分层数及无网格节点数下铝/氧化铝 Type B 方板中点归一化挠度 $\bar{w}^1$.从表 2 可知,当分层数为 1/12/1,节点布置数为 9×9 时,本文解已基本收敛,故对于 Type B 板中间核采用 12 层进行计算.表 3 给出了不同梯度指数 p 铝/氧化铝 Type B 方板中点归一化挠度 $\bar{w}^1$.从表 3 可知,本文解与采用 quasi-3D[34] 及反三角剪切变形理论(inverse trigonometric shear deformation theory,ITSDT)[35] 的数值解答较为相近,证明了本文方法计算 Type B 方板线性弯曲的准确性.表 4 给出了不同层状厚度与不同梯度指数 p 铝/氧化锆 Type C 方板中点归一化挠度 $\bar{w}^2$,可以看出,本文解与 FSDT[36] 所获得的数值解最大相对误差为 0.281%,证明了本文方法计算 Type C 方板线性弯曲的准确性.

表 2　分层数及节点数对铝/氧化铝方板中点归一化挠度 $\bar{w}^1$ 的影响($p = 10$, Type B)

Table 2　Effects of the numbers of layers and nodes on central deflection $\bar{w}^1$ of the Al/Al_2O_3 square plate ($p = 10$, Type B)

layers	present		
	5×5	9×9	13×13
1/4/1	0.829 7	0.826 1	0.826 1
1/8/1	0.864 8	0.861 0	0.861 0
1/12/1	0.861 9	0.858 0	0.858 0
1/16/1	0.860 8	0.857 0	0.857 0

表 3　不同梯度指数 p 下,铝/氧化铝方板中点归一化挠度 $\bar{w}^1$ (Type B)

Table 3　Normalized central deflection $\bar{w}^1$ for the Al/Al_2O_3 square plate with different gradient indices p (Type B)

method	p				
	0	0.5	1	4	10
Nguyen et al.[35] (ITSDT)	0.374 4	0.524 5	0.634 5	0.833 1	0.880 7
Neves et al.[34] (quasi-3D)	0.371 1	0.523 8	0.630 5	0.819 9	0.864 5
present	0.374 9	0.523 1	0.632 2	0.819 8	0.858 0

4.3　Type A 和 Type B 柱壳

如图 6(a)和 6(b)所示,受径向均布荷载 $q = 1.0 \times 10^6$ N/m^{2}作用的 Type A 柱壳,边长 $a = 0.2$ m,弧度 $\theta = 0.2$ rad,半径 $R = 1$ m,厚度 $h = 0.01$ m.

表 5 讨论了梯度指数为 1,不同分层数及无网格节点数对四边简支 Type A 铝/氧化锆柱壳的中点挠度 $\bar{w}^3$ 的影响.表 6 给出了不同边界条件与不同梯度指数 p 下 Type A 铝/氧化锆柱壳中点归一化挠度 $\bar{w}^3$.由表 5 可知,当分层数为 8,无网格节点数为 13×13 时,采用本文方法分析此算例已基本收敛.从表 6 可知:本文获得的数值结果 0.060 30 与 Zhao 等[24] 采用 kp-Ritz 所解答的数值结果 0.060 72 相对误差为 0.692%,验证了本文方法计算 Type A 柱壳线性弯曲的准确性;Type A 铝/氧化锆柱壳中点挠度随着梯度指数 p 的增大而增大,随着边界约束的加强而减小.

表 4 不同层状厚度与不同梯度指数 p 下,铝/氧化锆方板中点归一化挠度 $\bar{w}^2$ (Type C)

Table 4 Normalized central deflection $\bar{w}^2$ for the Al/ZrO_2 square plate with different layer thicknesses and gradient indices p (Type C)

p	theory	1-0-1	2-1-2	1-1-1	2-2-1	1-2-1
1	Nguyen et al. [35] (ITSDT)	0.323 5	0.306 2	0.291 9	0.280 8	0.270 9
	Zenkour[36] (FSDT)	0.324 8	0.307 5	0.293 0	0.281 7	0.271 7
	Neves et al. [34] (quasi-3D)	–	0.307 0	0.292 9	0.282 0	0.272 2
	present	0.324 3	0.307 1	0.292 7	0.281 4	0.271 5
5	Nguyen et al. [35] (ITSDT)	0.409 1	0.391 7	0.371 3	0.349 5	0.334 7
	Zenkour[36] (FSDT)	0.411 2	0.394 2	0.373 6	0.351 2	0.336 3
	Neves et al. [34] (quasi-3D)	–	0.390 5	0.370 5	0.349 0	0.334 7
	present	0.410 8	0.393 7	0.372 2	0.350 9	0.336 0
10	Nguyen et al. [35] (ITSDT)	0.417 5	0.403 9	0.385 4	0.362 0	0.348 2
	Zenkour[36] (FSDT)	0.419 2	0.406 6	0.387 9	0.364 0	0.350 0
	Neves et al. [34] (quasi-3D)	–	0.402 6	0.384 3	0.361 2	0.348 0
	present	0.418 9	0.406 2	0.387 5	0.363 6	0.349 7

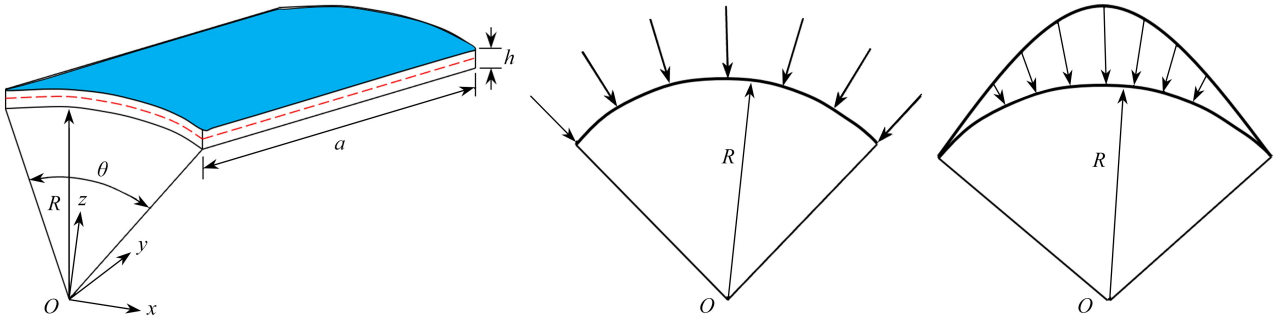

(a) 几何 (b) 径向均布荷载 (c) 径向正弦荷载

(a) Geometry (b) Radial uniformly distributed load (c) Radial sinusoidal load

图 6 功能梯度柱壳示意图

Fig. 6 Schematic diagram of a functionally graded cylindrical shell

表 5 分层数及节点数对四边简支铝/氧化锆柱壳中点挠度 $\bar{w}^3$ 的影响 (p = 1, Type A)

Table 5 Effects of the numbers of layers and nodes on central deflection $\bar{w}^3$ of the simply supported Al/ZrO_2 cylindrical shell (p = 1, Type A)

number of layers	present			
	5×5	9×9	13×13	17×17
4	0.060 76	0.060 07	0.060 10	0.060 12
8	0.060 97	0.060 29	0.060 30	0.060 34
12	0.061 01	0.060 33	0.060 36	0.060 38

表 6 不同边界条件与不同梯度指数 p 下,铝/氧化锆柱壳中点归一化挠度 $\bar{w}^3$ (Type A)

Table 6 Normalized central deflection $\bar{w}^3$ for the Al/ZrO_2 cylindrical shell with different boundary conditions and gradient indices p (Type A)

B.Cs	method	p					
		0	0.2	0.5	1	2	5
SSSS	kp-Ritz[24]	0.042 67	0.048 07	0.054 25	0.060 72	0.066 58	0.072 35
	present	0.042 47	0.047 69	0.053 80	0.060 30	0.066 37	0.072 46
CCCC	kp-Ritz[24]	0.013 47	0.015 16	0.017 11	0.019 15	0.021 02	0.022 89
	present	0.013 71	0.015 39	0.017 36	0.019 47	0.021 45	0.023 47

表 7 给出了不同径厚比 R/h 与不同梯度指数 p 四边简支 Type A 铝/氧化锆柱壳中点归一化挠度 $\bar{w}^3$.从

表 7 可知:同曲率半径的铝/氧化锆柱壳中点挠度随着梯度指数 p 的增大而增大;同梯度指数的铝/氧化锆柱壳中点挠度随着半径的增大而增大.这是因为随着半径的增大,柱壳已慢慢趋近于一个板结构,柱壳膜力慢慢减少,导致其挠度增大.

表 7　不同径厚比 R/h 与不同梯度指数 p 下,四边简支铝/氧化锆柱壳中点归一化挠度 $\bar{w}^3$ (Type A)

Table 7　Normalized central deflection $\bar{w}^3$ for the simply supported Al/ZrO_2 cylindrical shell with different radius-to-thickness ratios R/h and gradient indices p (Type A)

p	R/h	method				
		FSDT[37]	CST[37]	analytical[38]	kp-Ritz[24]	present
1	50	0.004 24	0.004 08	0.004 30	0.004 28	0.004 25
	100	0.060 56	0.060 02	0.060 91	0.060 72	0.060 30
	200	0.725 84	0.724 70	0.727 10	0.728 30	0.722 21
2	50	0.004 64	0.004 46	0.004 70	0.004 69	0.004 67
	100	0.066 40	0.065 78	0.066 79	0.066 78	0.066 37
	200	0.803 07	0.801 73	0.805 60	0.805 70	0.801 18

如图 6(a)和 6(c)所示,受径向正弦荷载作用的四边简支 Type B 铝/氧化铝柱壳,厚度类型为 1-8-1.正弦荷载 $q(r_1, r_2) = q\sin(\pi r_1/a)\sin(\pi r_2/b)$,$q = 1$ Pa,$R = 10$ m,$a = 1$ m,$\theta = 60°$.

表 8 给出了不同分层数及无网格节点数对四边简支 Type B 铝/氧化铝柱壳中点挠度的影响.从表 8 可知,当分层数为 1/8/1,无网格节点数为 71×7 时,计算结果已基本收敛.其数值结果 $4.176\ 2\times10^{-8}$ m 与文献[39]中基于 FSDT 得到的结果 $4.224\ 5\times10^{-8}$ m 相对误差为 1.143%.据此,采用分层数 1/8/1 及无网格节点数 71×7 计算不同梯度指数及径厚比下 Type B 柱壳的中点挠度,本文解及相关文献解列于表 9.从表 9 可知,本文解与文献解数据较为吻合,证明了本文方法计算 Type B 柱壳线性弯曲的准确性.

表 8　分层数及节点数对四边简支 Type B 铝/氧化铝柱壳中点挠度 $w_c \times 10^{-11}$ 的影响,$p = 1$, $R/h = 1\ 000$ (单位: m)

Table 8　Effects of the numbers of layers and nodes on central deflection $w_c \times 10^{-11}$ for the simply supported Al/Al_2O_3 cylindrical shell, $p = 1$, $R/h = 1\ 000$, Type B (unit: m)

layers	present			
	31×3	51×5	71×7	91×9
1/4/1	3 946.5	4 155.7	4 172.5	4 173.7
1/8/1	3 950.7	4 159.2	4 176.2	4 177.1
1/12/1	3 951.5	4 159.9	4 176.9	4 177.3

表 9　不同径厚比 R/h 与不同梯度指数 p 下,四边简支 Type B 铝/氧化铝柱壳中点挠度 $w_c \times 10^{-11}$ (单位: m)

Table 9　Normalized central deflection $w_c \times 10^{-11}$ for the simply supported Al/Al_2O_3 cylindrical shell with different radius-to-thickness ratios R/h and gradient indices p, Type B (unit: m)

p	method	R/h			
		4	10	100	1 000
1	CST[39]	0.004 6	0.066 1	55.428	4 223.3
	FSDT[39]	0.065 9	0.209 9	56.530	4 224.5
	present	0.064 8	0.208 7	56.420	4 176.2
5	CST[39]	0.006 1	0.086 4	73.651	6 578.3
	FSDT[39]	0.102 0	0.312 9	75.437	6 582.7
	present	0.098 9	0.310 5	75.120	6 579.8

4.4　Type A 双曲壳

如图 7 所示,承受均布荷载的四边简支 Type A 双曲壳 ($a = b$),其表达式为 $z = -(x^2/(2R_x) + xy/(2R_x) + y^2/(2R_y))$.可演变出 4 种不同壳体模型:(a) 柱壳 ($R_x = R$, $R_y = \infty$),(b) 球壳 ($R_x = R_y = R$),(c) 双曲抛物面壳 ($R_x = R$, $R_y = -R$),(d) 椭圆抛物面壳 ($R_x = R$, $R_y \neq R$).

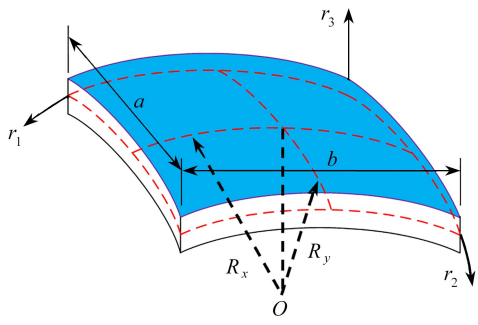

图 7 双曲壳几何模型

Fig. 7 Geometry of a doubly-curved functionally graded shell

表 10 给出了梯度指数为 1,分层数及节点数对四边简支铝/氧化铝柱壳中点挠度 $\bar{w}^4$ 的收敛情况.分析发现,当分层数为 12,节点数为 13×13 时,可认为采用本文方法分析此算例已基本收敛.其数值结果 8.920 9 与 Sayyad 等[37]基于 Navier 解答中的 FSDT 数值结果 8.907 2 相对误差为 0.154%,证明了本文方法计算 Type A 柱壳线性弯曲的准确性.据此,选取分层数 12 和节点数 13×13 计算后续 Type A 双曲壳算例.

表 11 分别给出了不同梯度指数 p 下,四边简支铝/氧化铝不同形状壳无量纲中点挠度 $\bar{w}^4$.p = 2 和 R_x/a = 5 的四边简支铝/氧化铝不同形状壳挠度云图如图 8 所示.分析表 11 可知:本文方法在分析各类不同形状 Type A 经典壳体时都具有较好的准确性,同时又体现了本文计算方法计算精度高这一特征;在同等曲率半径及梯度指数下,球壳挠度相比其他三种经典壳体较小,说明球壳形抵抗能力更强,膜力更大;随着功能梯度指数增大,弹性模量减小,整个结构刚度减小,导致其挠度增大.

表 10 分层数及节点数对四边简支铝/氧化铝柱壳中点挠度 $\bar{w}^4$ 的影响

Table 10 Effects of the numbers of layers and nodes on central deflection $\bar{w}^4$ of the simply supported Al/Al_2O_3 cylindrical shell

layers	present			
	5×5	9×9	13×13	17×17
4	8.873 9	8.762 6	8.759 9	8.760 0
8	9.010 0	8.897 0	8.894 3	8.894 4
12	9.036 3	8.923 0	8.920 2	8.920 4
16	9.045 6	8.932 1	8.929 4	8.929 5

表 11 不同梯度指数 p 下,四边简支铝/氧化铝不同形状壳中点归一化挠度 $\bar{w}^4$

Table 11 Normalized central deflection $\bar{w}^4$ for the simply supported Al/Al_2O_3 different shells with various gradient indices p

shell type	method	p				
		0	1	5	10	∞
cylindrical shell (R_x/a = 5, R_y/b = ∞)	ESDT[37]	4.526 5	8.964 8	13.942 0	15.460 0	24.572 0
	FSDT[37]	4.492 1	8.907 2	13.683 0	15.152 0	24.385 0
	present	4.525 5	8.920 2	13.827 4	15.401 0	24.567 1
spherical shell (R_x/a = 5, R_y/b = 5)	ESDT[37]	4.157 1	8.119 3	12.816 0	14.333 0	22.567 0
	FSDT[37]	4.128 5	8.072 9	12.601 0	14.071 0	22.412 0
	present	4.161 1	8.073 9	12.699 3	14.268 6	22.588 9
hyperbolic paraboloid shell (R_x/a = 5, R_y/b = −5)	ESDT[37]	4.664 6	9.286 8	14.362 0	15.876 0	25.322 0
	FSDT[37]	4.627 8	9.224 6	14.086 0	15.550 0	25.122 0
	present	4.653 9	9.239 8	14.250 7	15.815 4	25.263 9
elliptical paraboloid shell (R_x/a = 5, R_y/b = 7.5)	ESDT[37]	4.300 3	8.444 2	13.253 0	14.772 0	23.344 0
	FSDT[37]	4.269 4	8.393 7	13.021 0	14.493 0	23.177 0
	present	4.303 0	8.399 1	13.136 1	14.709 9	23.359 2

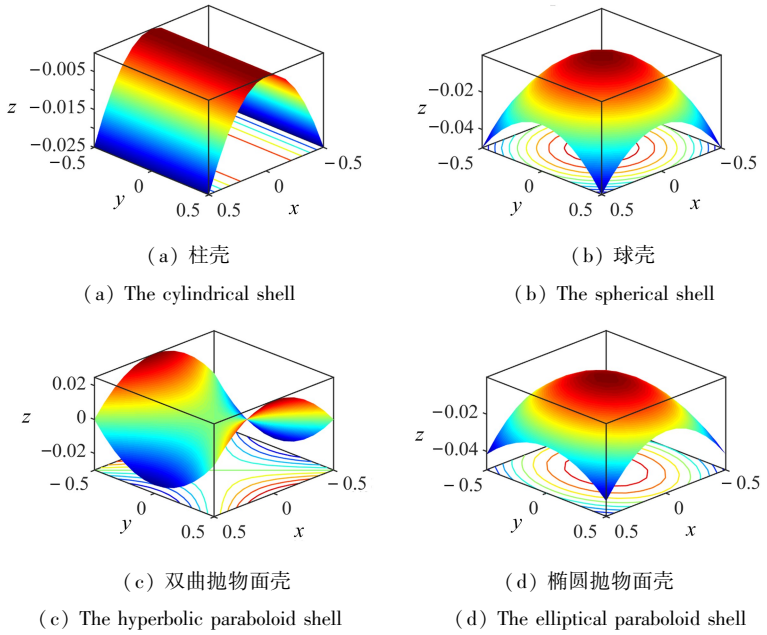

(a) 柱壳　　(b) 球壳

(a) The cylindrical shell　　(b) The spherical shell

(c) 双曲抛物面壳　　(d) 椭圆抛物面壳

(c) The hyperbolic paraboloid shell　　(d) The elliptical paraboloid shell

图 8　梯度指数为 2 和 $R_x/a = 5$ 的四边简支铝/氧化铝不同形状壳挠度云图(EFG)

Fig. 8　Deflection neghogram for the simply supported Al/Al_2O_3 different shape shells with gradient indices $p = 2$ and $R_x/a = 5$(EFG)

5　结　　论

本文基于 3D 连续壳及分层理论,结合一阶剪切变形理论,提出了一种求解功能梯度三明治壳线性弯曲的移动最小二乘近似无网格法.通过计算几个不同功能梯度类型板壳算例,并将计算结果与文献解进行对比,得出了以下结论:

1) 本文方法具有较好的收敛性,虽不能完全避免剪切锁死现象,但可通过提高基函数阶次和适当扩大影响域来消除剪切锁死.

2) 本文解与文献解极为相近,验证了本文方法计算功能梯度三明治壳线性弯曲的有效性及准确性.

3) 由于本文提出的求解功能梯度三明治壳线性弯曲问题的无网格模型不含广义壳体理论中的 Lamé 系数项,本文方法还可适用于任意空间曲面的功能梯度三明治壳,如变曲率、非正交曲线坐标系统等壳体.

参考文献(References):

[1] KOIZUMI M. The concept of FGM[J]. *Ceramic Transactions*, 1993, **34**: 3-10.

[2] 沈惠申. 功能梯度复合材料板壳结构的弯曲、屈曲和振动[J]. 力学进展, 2004, **34**(1): 53-60.(SHEN Huishen. Bending, buckling and vibration of functionally graded plates and shells[J]. *Advances in Mechanics*, 2004, **34**(1): 53-60. (in Chinese))

[3] LIEW K M, ZHAO X, FERREIRA A J M. A review of meshless methods for laminated and functionally graded plates and shells[J]. *Composite Structures*, 2011, **93**(8): 2031-2041.

[4] 李尧臣, 亓峰, 仲政. 功能梯度矩形板的近似理论与解析解[J]. 力学学报, 2010, **42**(4): 670-681.(LI Yaochen, QI Feng, ZHONG Zheng. Approximation theory and analytical solution for functionally graded piezoelectric rectangular plates[J]. *Chinese Journal of Theoretical and Applied Mechanics*, 2010, **42**(4): 670-681. (in Chinese))

[5] WOODWARD B, KASHTALYAN M. Three-dimensional elasticity solution for bending of transversely isotropic functionally graded plates[J]. *European Journal of Mechanics A: Solids*, 2011, **30**(5): 705-718.

[6] 沈璐璐, 蔡方圆, 杨博. 功能梯度压电板柱面弯曲的弹性力学解[J]. 应用数学和力学, 2023, **44**(3): 272-281.

(SHEN Lulu, CAI Fangyuan, YANG Bo. Elastic solutions for cylindrical bending of functionally graded piezoelectric material plates[J]. *Applied Mathematics and Mechanics*, 2023, **44**(3): 272-281. (in Chinese))

[7] 张靖华, 李世荣, 马连生. 功能梯度截顶圆锥壳的热弹性弯曲精确解[J]. 力学学报, 2008, **40**(2): 185-193. (ZHANG Jinghua, LI Shirong, MA Liansheng. Exact solution of thermoelastic bending for functionally graded truncated conical shells[J]. *Chinese Journal of Theoretical and Applied Mechanics*, 2008, **40**(2): 185-193. (in Chinese))

[8] PAYETTE G S, REDDY J N. A seven-parameter spectral/*hp* finite element formulation for isotropic, laminated composite and functionally graded shell structures[J]. *Computer Methods in Applied Mechanics and Engineering*, 2014, **278**: 664-704.

[9] PARAND A A, ALIBEIGLOO A. Static and vibration analysis of sandwich cylindrical shell with functionally graded core and viscoelastic interface using DQM[J]. *Composites*(*Part B*): *Engineering*, 2017, **126**: 1-16.

[10] 刘涛, 李朝东, 汪超, 等. 基于三阶剪切变形理论的压电功能梯度板静力学等几何分析[J]. 振动与冲击, 2021, **40**(1): 73-85.(LIU Tao, LI Chaodong, WANG Chao, et al. Static iso- geometric analysis of piezoelectric functionally graded plate based on third-order shear deformation theory[J]. *Journal of Vibration and Shock*, 2021, **40**(1): 73-85. (in Chinese))

[11] 黄干云, 汪越胜, 余寿文. 功能梯度材料的平面断裂力学分析[J]. 力学学报, 2005, **37**(1): 1-8.(HUANG Ganyun, WANG Yuesheng, YU Shouwen. A new multi-layered model for in-plane fracture analysis of functionally graded materials[J]. *Chinese Journal of Theoretical and Applied Mechanics*, 2005, **37**(1): 1-8. (in Chinese))

[12] WANG Y S, HUANG G Y, GROSS D. On the mechanical modeling of functionally graded interfacial zone with a Griffith crack: anti-plane deformation[J]. *International Journal of Fracture*, 2003, **125**(3): 189-205.

[13] 黄立新, 姚祺, 张晓磊, 等. 基于分层法的功能梯度材料有限元分析[J]. 玻璃钢/复合材料, 2013(2): 43-48. (HUANG Lixin, YAO Qi, ZHANG Xiaolei, et al. Finite element analysis of functionally graded materials based on layering method[J]. *Composite Science and Engineering*, 2013(2): 43-48. (in Chinese))

[14] NIKBAKHT S, SALAMI S J, SHAKERI M. Three dimensional analysis of functionally graded plates up to yielding, using full layer-wise finite element method[J]. *Composite Structures*, 2017, **182**: 99-115.

[15] BRISCHETTO S. A 3D layer-wise model for the correct imposition of transverse shear/normal load conditions in FGM shells[J]. *International Journal of Mechanical Sciences*, 2018, **136**: 50-66.

[16] 龙述尧, 刘凯远, 李光耀. 功能梯度材料中的无网格局部径向点插值法[J]. 湖南大学学报(自然科学版), 2007, **34**(3): 41-44.(LONG Shuyao, LIU Kaiyuan, LI Guangyao. A meshless local radial point interpolation method for the analysis of functionally graded materials[J]. *Journal of Hunan University* (*Natural Sciences*), 2007, **34**(3): 41-44. (in Chinese))

[17] 邵玉龙, 段庆林, 李锡夔, 等. 功能梯度材料的二阶一致无网格法[J]. 工程力学, 2017, **34**(3): 15-21.(SHAO Yulong, DUAN Qinlin, LI Xikui, et al. Quadratically consistent meshfree method for functionally graded materials[J]. *Engineering Mechanics*, 2017, **34**(3): 15-21. (in Chinese))

[18] QIAN L F, BATRA R C, CHEN L M. Static and dynamic deformations of thick functionally graded elastic plates by using higher-order shear and normal deformable plate theory and meshless local Petrov-Galerkin method[J]. *Composites*(*Part B*): *Engineering*, 2004, **35**: 685-697.

[19] LEE Y Y, ZHAO X, LIEW K M. Thermoelastic analysis of functionally graded plates using the element-free kp-Ritz method[J]. *Smart Materials and Structures*, 2009, **18**(3): 035007.

[20] THAI C H, DO V N V, NGUYEN-XUAN H. An improved moving Kriging-based meshfree method for static, dynamic and buckling analyses of functionally graded isotropic and sandwich plates[J]. *Engineering Analysis With Boundary Elements*, 2016, **64**: 122-136.

[21] HOSSEINI S, RAHIMI G, ANANI Y. A meshless collocation method based on radial basis functions for free and forced vibration analysis of functionally graded plates using FSDT[J]. *Engineering Analysis With Boundary Elements*, 2021, **125**: 168-177.

[22] VU T V, KHOSRAVIFARD A, HEMATIYAN M R, et al. Enhanced meshfree method with new correlation functions for functionally graded plates using a refined inverse sin shear deformation plate theory[J]. *European Journal of Mechanics A: Solids*, 2019, **74**: 160-175.

[23] SLADEK J, SLADEK V, ZHANG C, et al. Static and dynamic analysis of shallow shells with functionally graded and orthotropic material properties[J]. *Mechanics of Advanced Materials and Structures*, 2008, **15**(2): 142-156.

[24] ZHAO X, LEE Y Y, LIEW K M. Thermoelastic and vibration analysis of functionally graded cylindrical shells [J]. *International Journal of Mechanical Sciences*, 2009, **51**(9/10): 694-707.

[25] ZHAO X, LIEW K M. A mesh-free method for analysis of the thermal and mechanical buckling of functionally graded cylindrical shell panels[J]. *Computational Mechanics*, 2010, **45**: 297-310.

[26] ZHAO X, LIEW K M. Free vibration analysis of functionally graded conical shell panels by a meshless method [J]. *Composite Structures*, 2011, **93**(2): 649-664.

[27] MELLOULI H, JRAD H, WALI M, et al. Meshfree implementation of the double director shell model for FGM shell structures analysis[J]. *Engineering Analysis With Boundary Elements*, 2019, **99**: 111-121.

[28] SIMO J C, FOX D D, RIFAI M S. Formulation and computational aspects of a stress resultant geometrically exact shell model[J]. *Computation Mechanics*, 1990, **55**: 751-759.

[29] WANG L, LIU Y, ZHOU Y, et al. Static and dynamic analysis of thin functionally graded shell with in-plane material inhomogeneity[J]. *International Journal of Mechanical Sciences*, 2021, **193**: 106165.

[30] AHMAD S, IRONS B M, ZIENKIEWICZ O C. Analysis of thick and thin shell structures by curved finite elements[J]. *International Journal for Numerical Methods in Engineering*, 1970, **2**: 419-451.

[31] SALKAUSKAS P L. Surfaces generated by moving least squares methods[J]. *Mathematics of Computation*, 1981, **37**(155): 141-158.

[32] CHEN J S, PAN C, WU C T, et al. Reproducing kernel particle methods for large deformation analysis of nonlinear structures[J]. *Computer Methods in Applied Mechanics and Engineering*, 1996, **139**(4): 195-227.

[33] TIMOSHENKO S. *Theory of Plates and Shells*[M]. New York: McGraw-Hill Book Company, 1959.

[34] NEVES A M A, FERREIRA A J M, CARRERA E, et al. Static, free vibration and buckling analysis of isotropic and sandwich functionally graded plates using a quasi-3D higher-order shear deformation theory and a meshless technique[J]. *Composites(Part B): Engineering*, 2013, **44**(1): 657-674.

[35] NGUYEN V H, NGUYEN T K, THAI H T, et al. A new inverse trigonometric shear deformation theory for isotropic and functionally graded sandwich plates[J]. *Composites(Part B): Engineering*, 2014, **66**: 233-246.

[36] ZENKOUR A M. A comprehensive analysis of functionally graded sandwich plates, part 1: deflection and stresses[J]. *International Journal of Solids and Structures*, 2005, **42**(18): 5224-5242.

[37] SAYYAD A S, GHUGAL Y M. Static and free vibration analysis of doubly-curved functionally graded material shells[J]. *Composite Structures*, 2021, **269**: 114045.

[38] HUAN D T, TU T M, QUOC T H. Analytical solutions for bending, buckling and vibration analysis of functionally graded cylindrical panel[J]. *Vietnam Journal of Science Technology*, 2017, **55**(5): 587-597.

[39] CARRERA E, BRISCHETTO S, CINEFRA M, et al. Effects of thickness stretching in functionally graded plates and shells[J]. *Composites(Part B): Engineering*, 2011, **42**(2): 123-133.